

1. Optimization of parameters for nanoSIMS measurement

In order to get a considerable precision in isotopic composition at single-cell level, the nanoSIMS measurement parameters were optimized prior the analysis of isotope-labelled samples.

P. stutzeri cells were prepared as explained in material and methods section for nanoSIMS analysis. Cells prior labelling were analyzed in order to avoid further effect of single cell variability in ^{13}C uptake. Therefore, single-cell precision of the derived isotope content was evaluated at the level of natural ^{13}C abundance.

Analysis of single-cell isotopic content was performed using a NanoSIMS 50L instrument (AMETEK, Cameca) detecting 7 secondary molecular ion species: $^{16}\text{O}^-$, $^{12}\text{C}_2^-$, $^{13}\text{C}^{12}\text{C}^-$, $^{12}\text{C}^{14}\text{N}^-$, $^{13}\text{C}^{14}\text{N}^-$, $^{32}\text{S}^-$ and $^{31}\text{P}^{16}\text{O}_2^-$. For the optimization, two main parameters were tuned: primary ion (PI) current and analyzed area size. The ability to focus the PI beam down to 30 nm resolution is usually achieved with the reduction of the beam current. In the present study, the nanoSIMS performance has been tested with 2 different values of PI current: 2 and 4 pA in order to clarify the possibility of speeding-up the measurement and enhancing counting statistics with higher secondary ion counts compromising the focus quality. Different sizes of analysis area were checked to reach an optimal pixel-count statistics for each single-cell-RoI with an acceptable number of single-cells resolved in the analyzed Field of View (FoV).

Prior to analysis, filter areas of $100 \times 100 \mu\text{m}^2$ were pre-implanted with primary ions beam Cesium (Cs^+) at 100 pA for 5 minutes. The number of pixels per single-cell can be tuned by changing the size of analyzed area keeping constant the raster size (512×512 pixels); therefore, 40×40 , 30×30 and $20 \times 20 \mu\text{m}^2$ area were analyzed for the optimization. The dwell time was fixed to 2 ms/pixel for the whole optimization procedure.

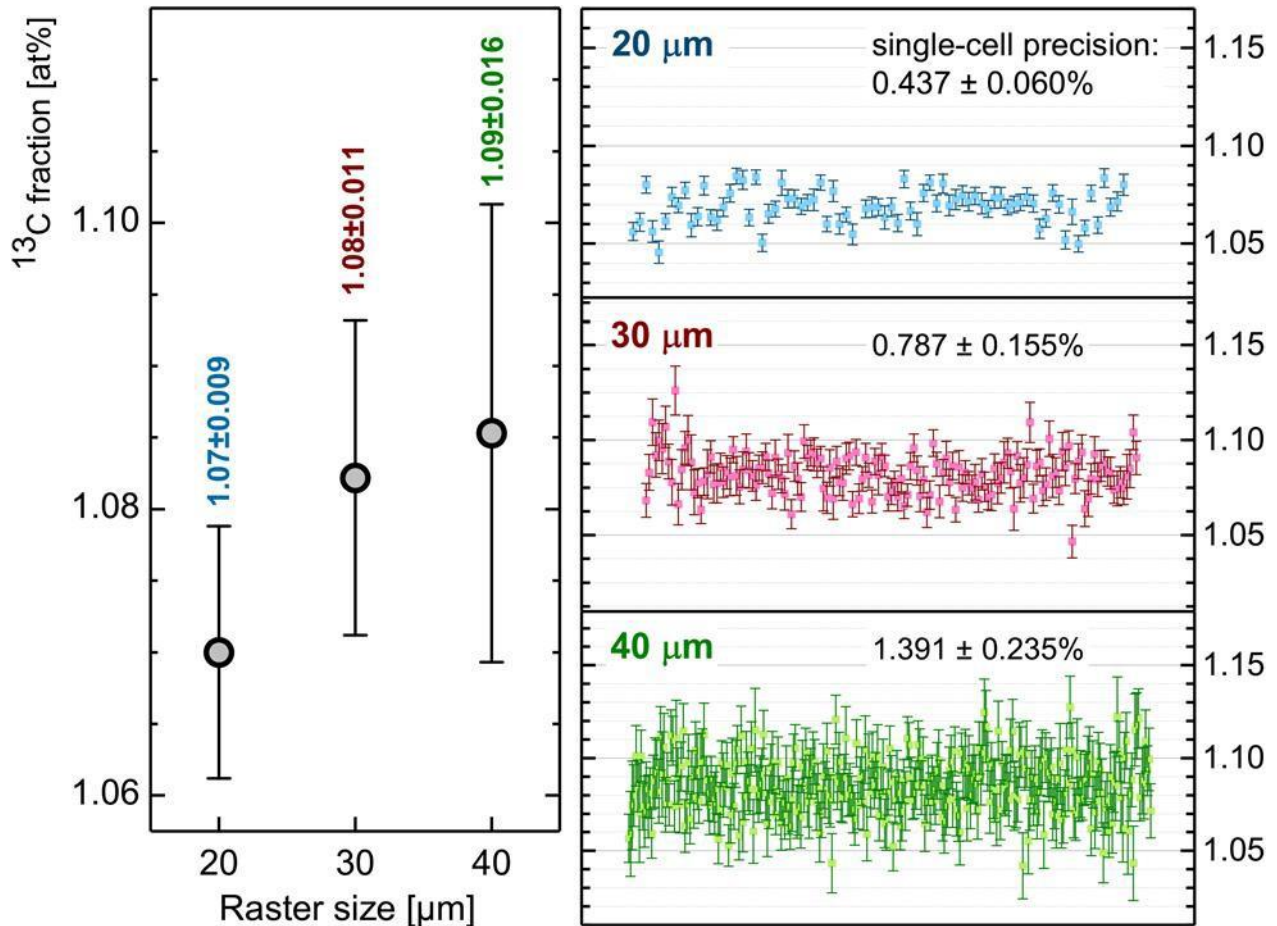
The settings with 2 pA PI current was tested (Fig. S1) first to verify the influence of pixel number per single cell on the precision of single-cell derived isotope fraction. The best precision of isotope fraction at single-cell level was achieved for 2 pA PI current with $20 \times 20 \mu\text{m}^2$ analysis area ($0.44 \pm 0.06\%$, mean of single-cell σ over isotope-fraction for all single-cells measured) due to maximal number of pixels per single-cell obtained with the smallest pixel size (39 nm versus 58 nm and 78 nm with 30 μm and 40 μm raster, respectively). With 2 pA PI current and $40 \times 40 \mu\text{m}^2$ analysis area, the relative error of single-cell isotope fraction reached $1.39 \pm 0.24\%$; therefore, this size of analysis area was not considered for further optimization. For the $30 \times 30 \mu\text{m}^2$ analysis area, the relative error was $0.79 \pm 0.16\%$ with 2 pA PI current.

PI beam current of 4 pA (Fig. S2) with $30 \times 30 \mu\text{m}^2$ analysis area resulted in $0.88 \pm 0.14\%$ precision of isotope fraction at single-cell level. The analysis settings with 4 pA PI current and $20 \times 20 \mu\text{m}^2$ analysis area were selected providing a considerable analysis speed and $0.37 \pm 0.05\%$ relative error of isotopic content at single-cell level. In this condition, the highest pixel density with sufficient secondary ion counts per pixel (consequently better ion-count statistics for single-cells) and a considerable quality of PI beam focusing were achieved.

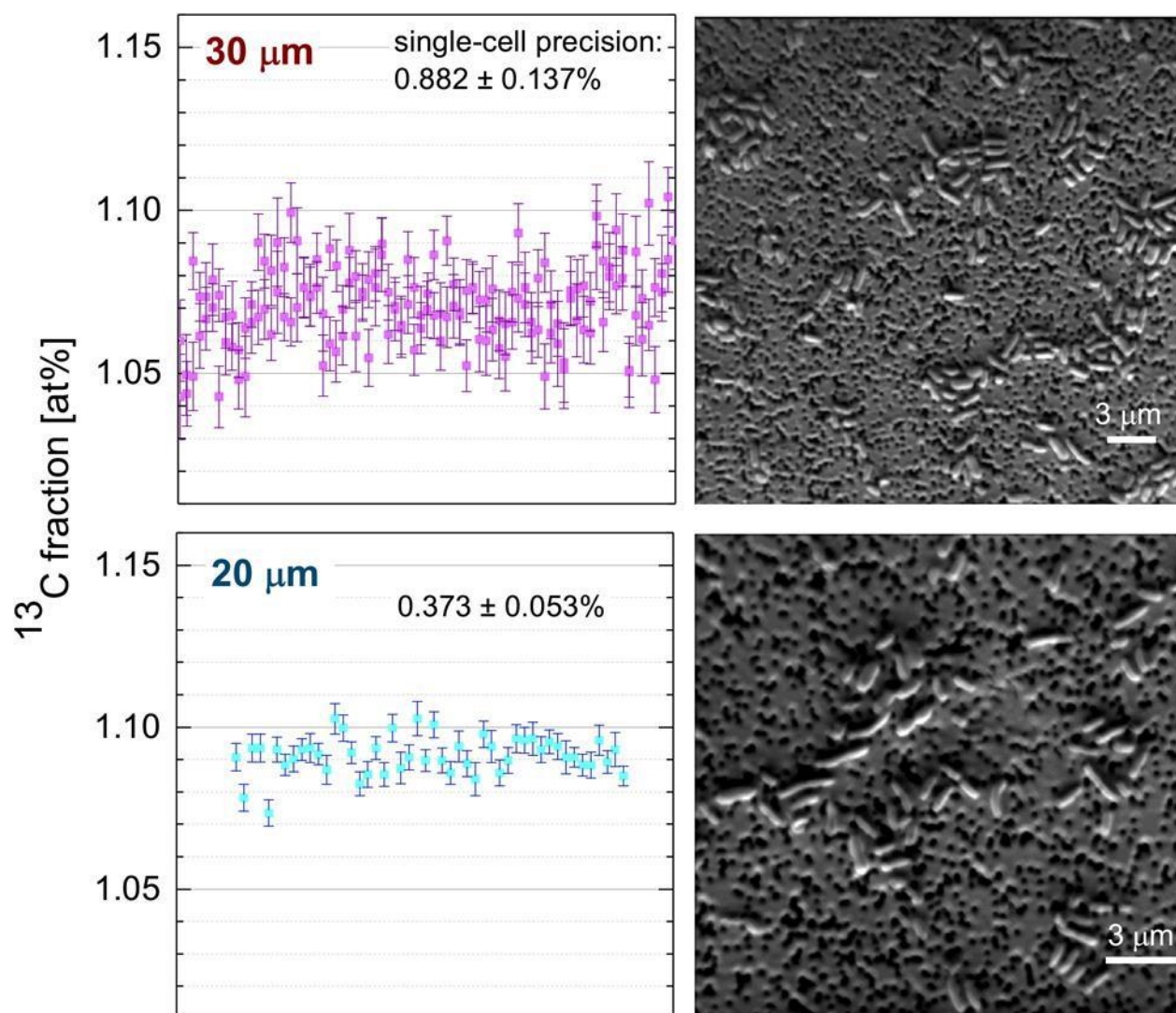
NanoSIMS data acquired for the optimization were processed with LANS (Polerecky et al., 2012); the single-cell RoI were drawn manually with the $^{12}\text{C}^{14}\text{N}^-$ map representing the biomass distribution.

The ^{13}C fraction ($D_{13\text{C}} \times 100$ [at%]) was evaluated from the ratio of C_2^- molecular ion counts ($R = N_{13\text{C}12\text{C}}/N_{12\text{C}12\text{C}}$) using the following expression:

$$D_{13\text{C}} = \frac{N_{13\text{C}12\text{C}}/N_{12\text{C}12\text{C}}}{\{2 \times (N_{13\text{C}12\text{C}}/N_{12\text{C}12\text{C}}) + 1\}} = \frac{R_{\text{C}_2}}{\{2 \times (R_{\text{C}_2} + 1)\}}$$



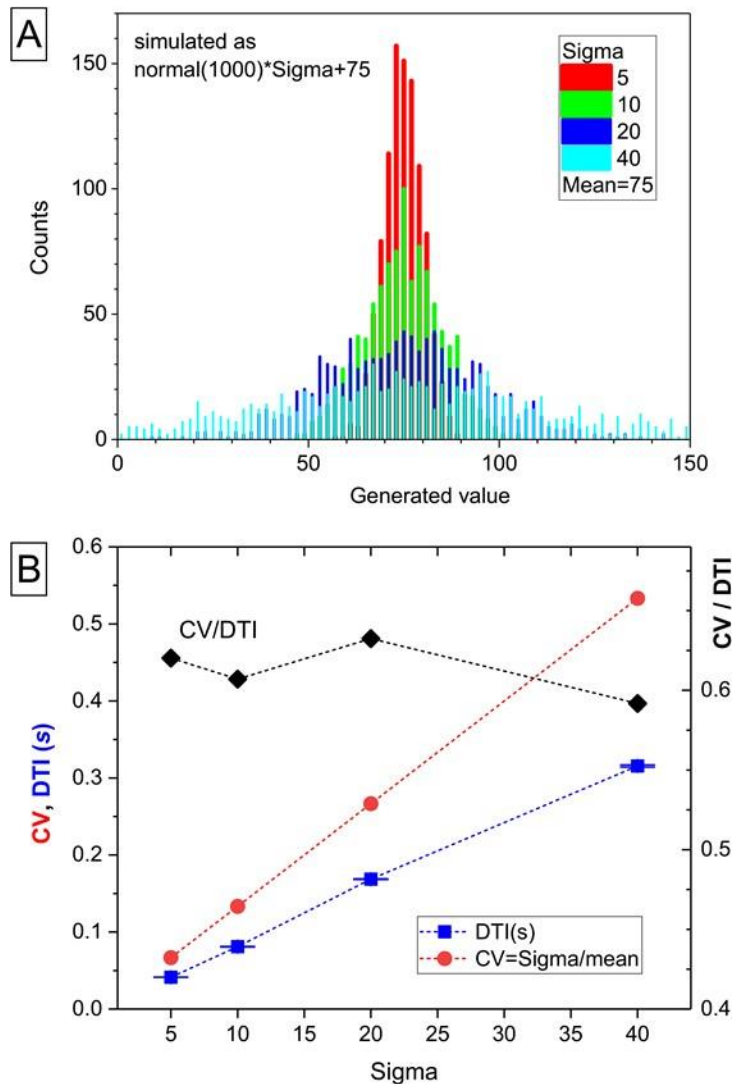
Supplementary Figure S1. Single-cell analysis of *P. stutzeri* cells. On the left panel mean value \pm SD achieved with three different sizes of sample areas analyzed with 2 pA primary ion current are shown. On the right panel, single-cell values of ^{13}C content are shown; symbols represent the ^{13}C fraction [at%] and its error ($\pm\sigma$, error bar) for each single-cell.



Supplementary Figure S2. Comparison of single-cell values of ^{13}C content and focus quality for $30 \times 30 \mu\text{m}^2$ and $20 \times 20 \mu\text{m}^2$ sample area (FoV) analyzed with 4 pA current of the primary Cs^+ ion beam.

2. Zipfian fit of normally-distributed data

The approximation of an experimental rank-activity distribution with $K_A(r; q, s, d, n)$ (Eq. 25 in the main text) provides a slope value s (Differentiation Tendency Index, DTI) characterizing the tendency of single-cell to differentiate in their anabolic activity. It has been assumed that when the rank-activity distribution of all cells inside a monoclonal population fit a single slope, then the cells follow unimodal activity. To prove the feasibility to measure heterogeneity in cellular activity with the slope of rank-activity distribution, simulated normal distributions (Figs. S3-A, S4) were approximated with the Zipfian function (Eq. 25).



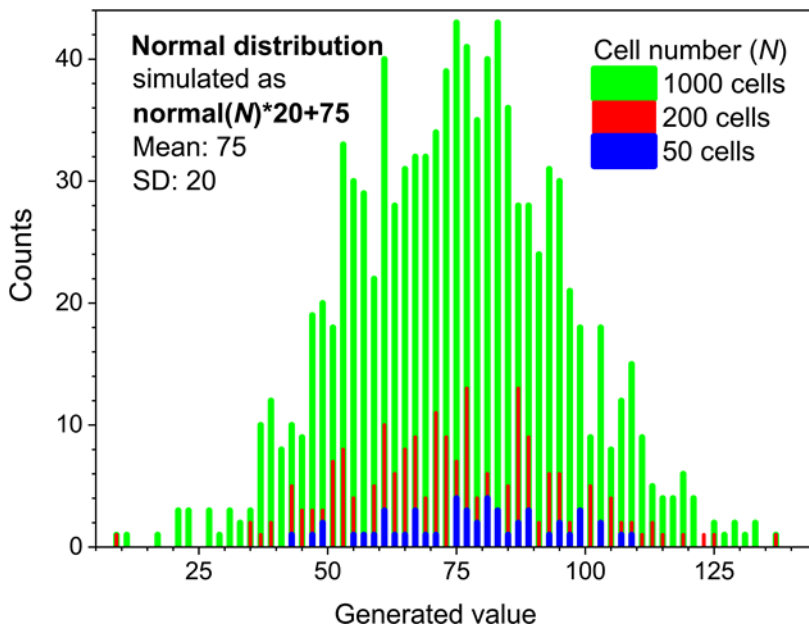
Supplementary Figure S3. Frame A: normal distribution simulated with fixed mean and different Sigma values. Frame B shows the DTI values derived as rank distribution slope with Zipfian fit ($s \pm \Delta s$, blue rectangles), corresponding CV values (red circles) and CV/DTI ratio calculated for different σ values with fixed the centroid (mean value) fixed at 75.

2.1. Correlation between Zipfian slope (DTI, s) and Coefficient of Variation (CV)

The DTI values, derived for the simulated normal distribution with fixed mean and different σ (Sigma; Standard Deviation, SD), were shown to reproduce the trend of corresponding CV values (Fig. S3-B) providing a proof for DTI as heterogeneity index.

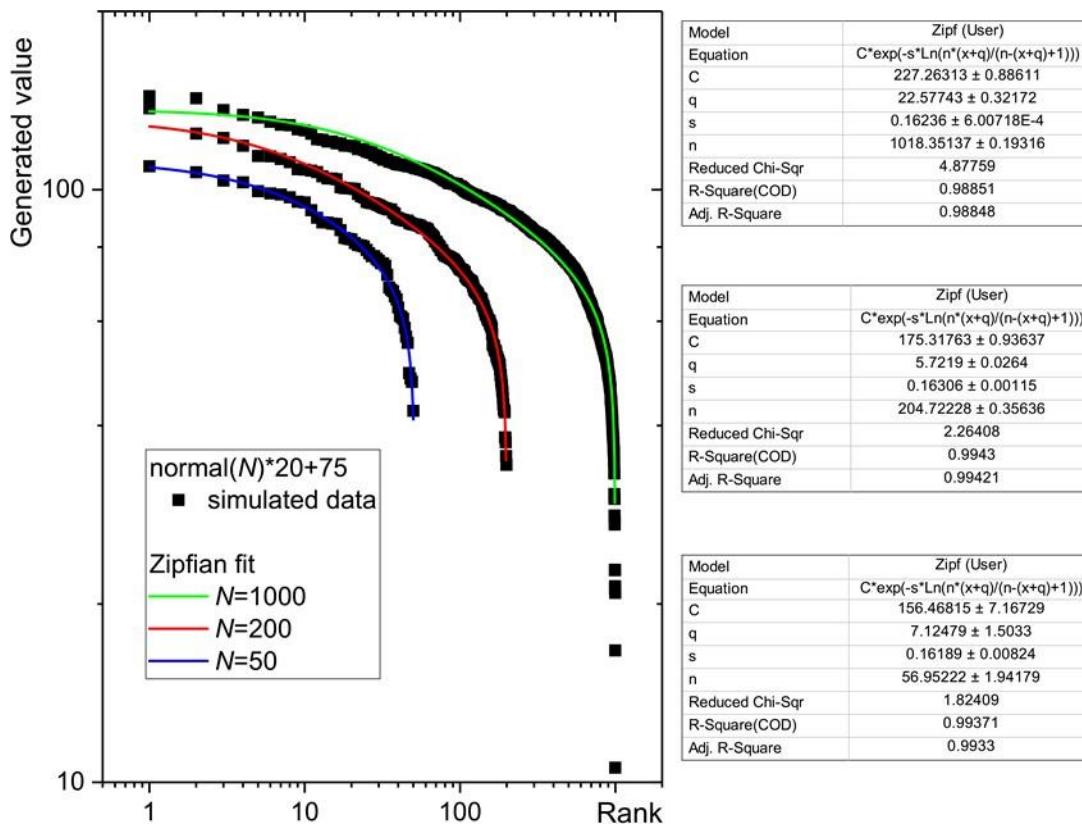
2.2. Invariance of Zipfian slope to population size

Normal cellular activity distributions were simulated with different population size (1000, 200 and 50 cells; Fig. S4) and the rank-activity distribution of simulated data were approximated with Zipfian function (Fig. S5). OriginPro 2017 software was used for data simulation and approximation of rank-activity distributions.



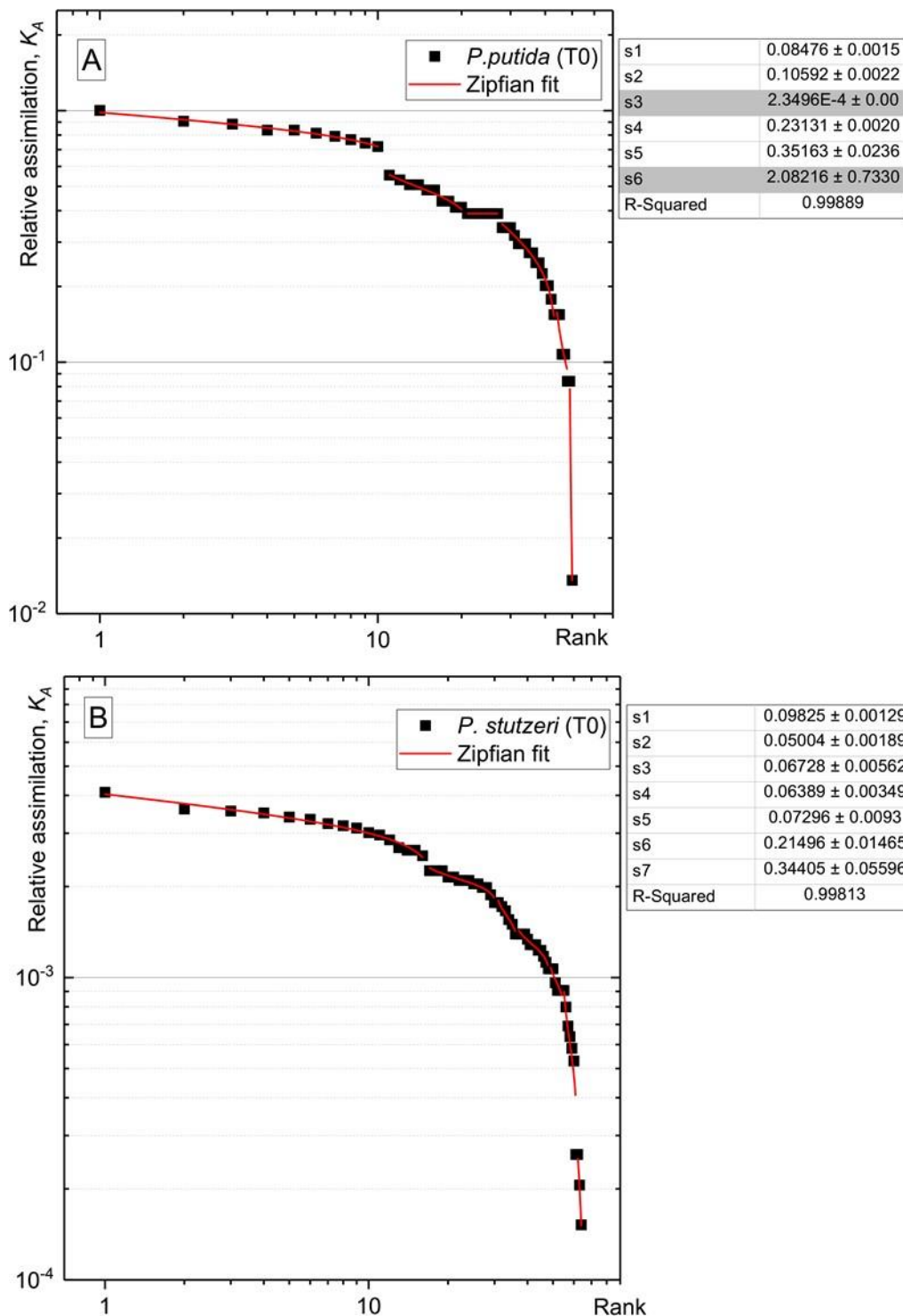
Supplementary Figure S4. Histograms plot of simulated normally distributed populations in single cell anabolic activity. The mean value and the SD (σ) were kept the same for different population size.

The approximation delivers the slope values (tables in Fig. S5) $s=0.1624\pm 0.0006$ for 1000 cells, $s=0.1631\pm 0.0011$ for 200 cells and $s=0.1619\pm 0.0082$ for 50 cells proving the invariance of s to the population size.

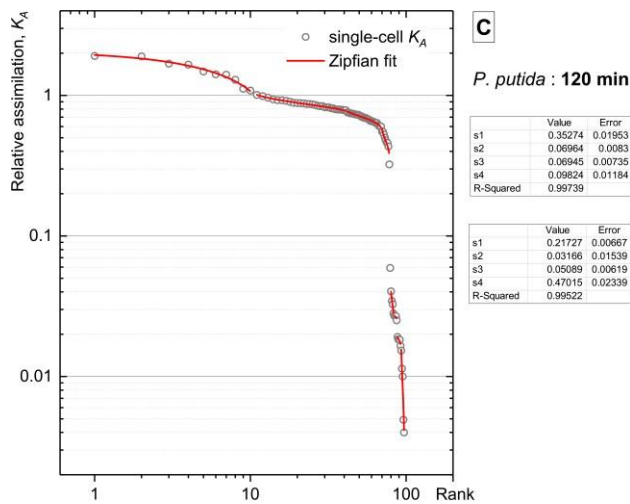
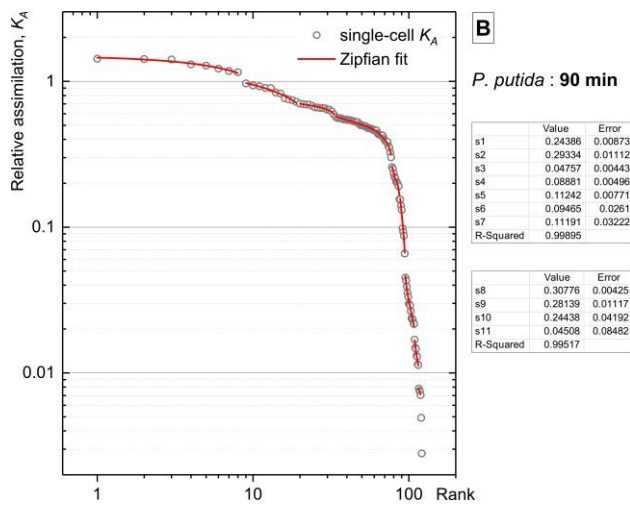
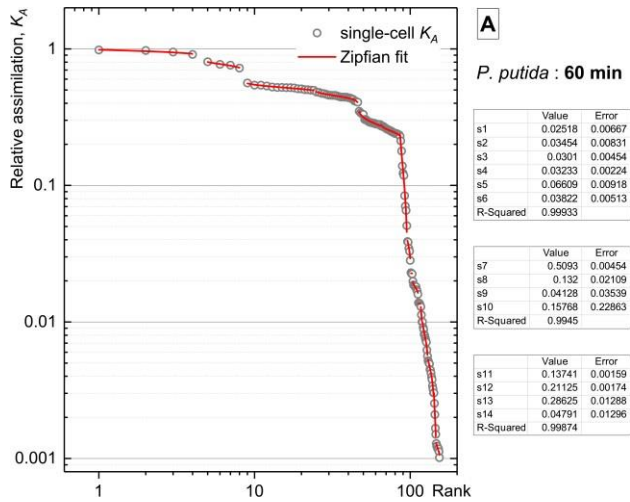


Supplementary Figure S5. Zipfian approximation of rank-activity distributions of cellular activity simulate for different population size (1000, 200 and 50 cells).

3. Zipfian approximation of rank-activity distribution

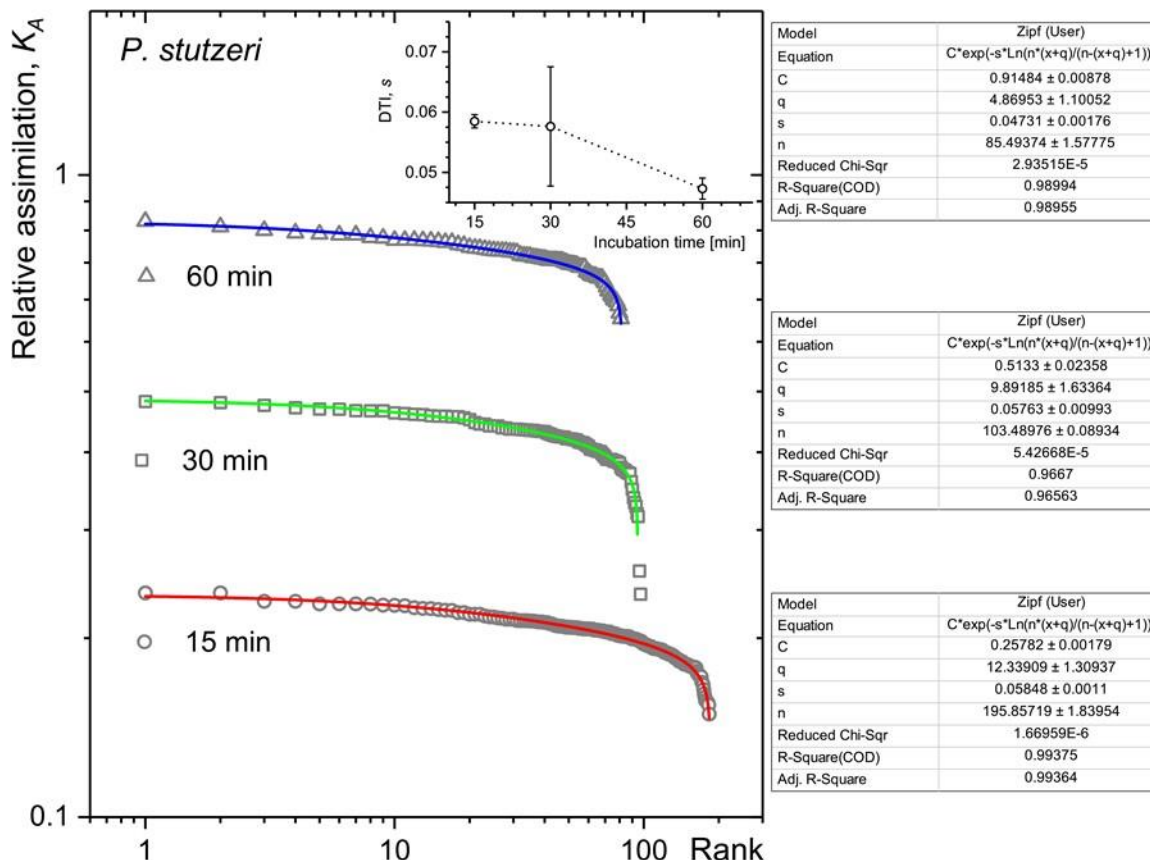


Supplementary Figure S6. Rank-activity distributions and multi-component Zipfian approximation of experimental data. Rank-activity distributions of *P. putida* (frame A) and *P. stutzeri* (frame B) at Time 0 approximated with multi-component Zipfian function (Eq. 26 in the main text). The tables on the right side show the fitted slope values ($s \pm \Delta s$) and R-squared representing fit accuracy.

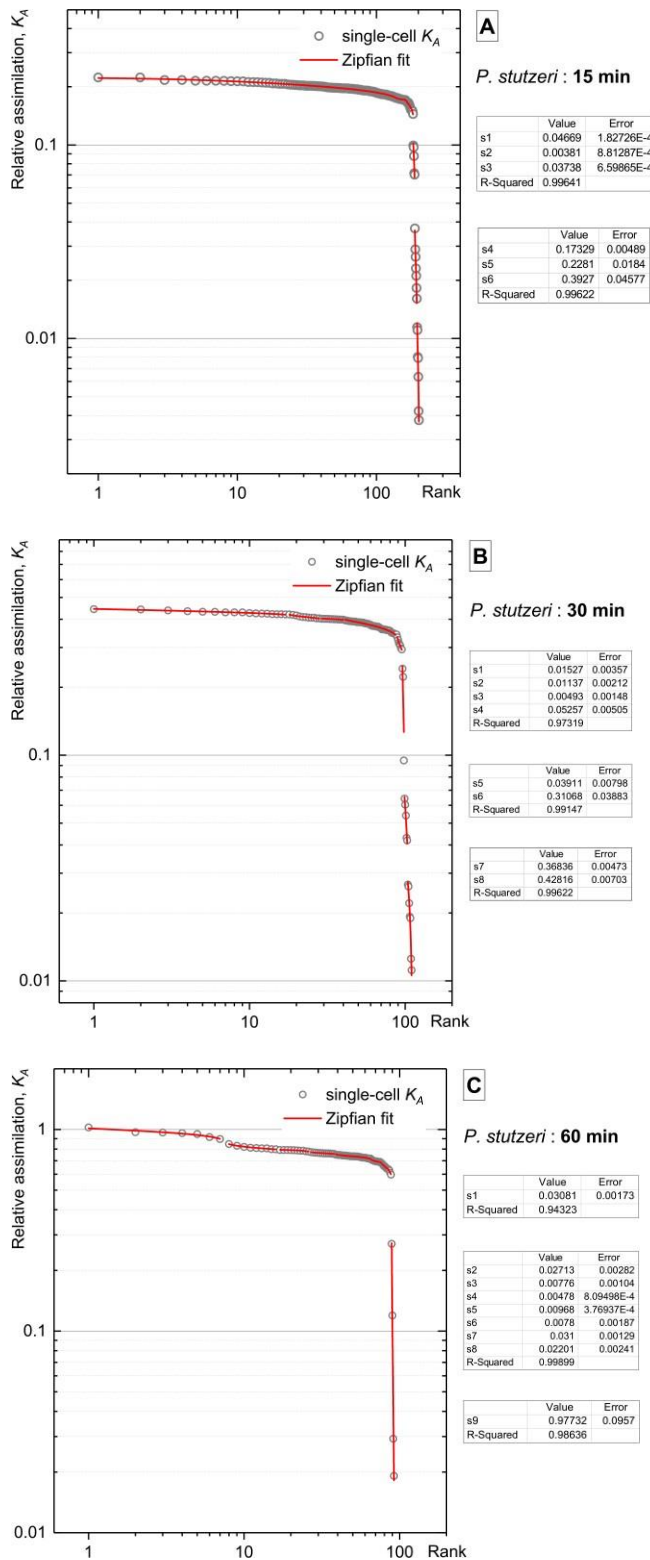


Supplementary Figure S7. Rank-activity distributions and multi-component Zipfian approximation for *P. putida* at different time points.

When cells reveal multimodal activity, their rank-activity distribution reveals steps assigned to subpopulations belonging to the same monoclonal population. Fit of a multimodal rank activity distribution with single-component Zipfian function (Eq. 25 in the main text) results in large relative [%] error in slope value ($\Delta s/s \times 100$ [%]) 1.9%, 17.2%, 3.7% for the 15, 30 and 60 minutes incubation time, respectively; Fig. S8). In such a case the multi-component Zipfian function has to be applied for data fit and CDTI ($S \pm \Delta S$, Eqs. 27, 28 in the main text) has to be derived to quantify the heterogeneity of entire population.

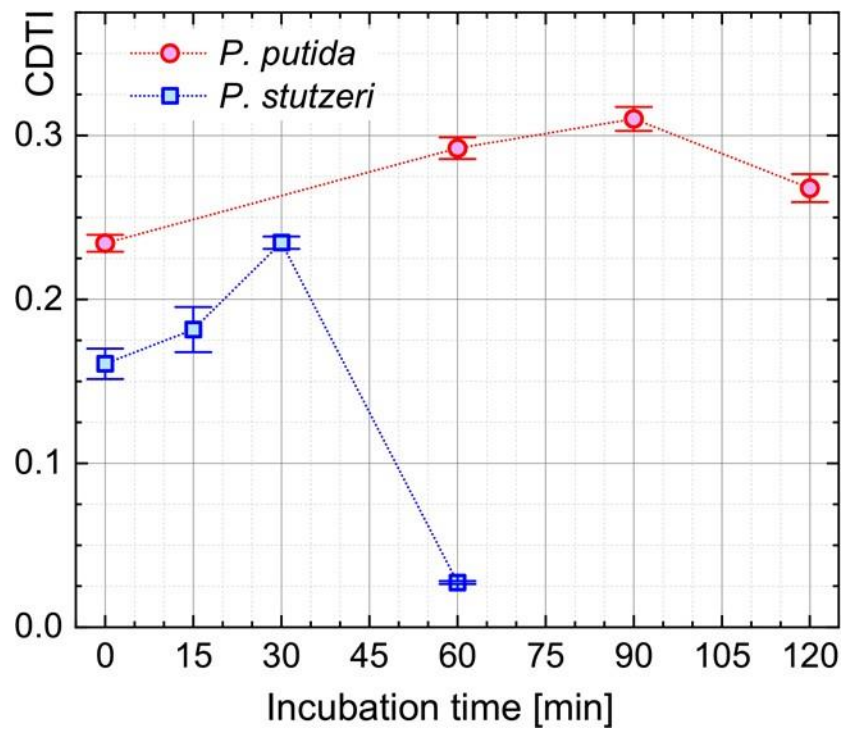


Supplementary Figure S8. Rank-activity distributions and single-component Zipfian approximation for *P. stutzeri* at different time points. The tables show the results of single-component Zipfian fit. The inset shows the $s \pm \Delta s$ obtained with the fit at different time points.

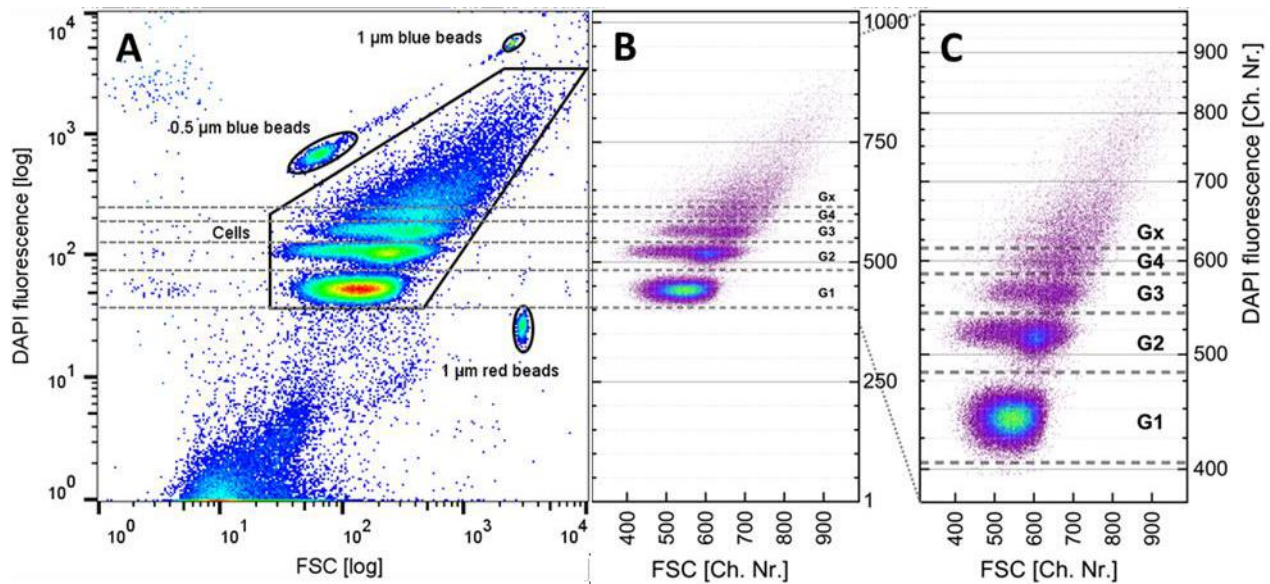


Supplementary Figure S9. Rank-activity distributions and multi-component Zipfian approximation for *P. stutzeri* at different time points. At time point 60 minutes (frame C), 4 cells were initially assigned to a low-SDT subpopulation. However, such cells, distributed over one order of magnitude of their K_A values, could not be further considered as a single subpopulation and were therefore

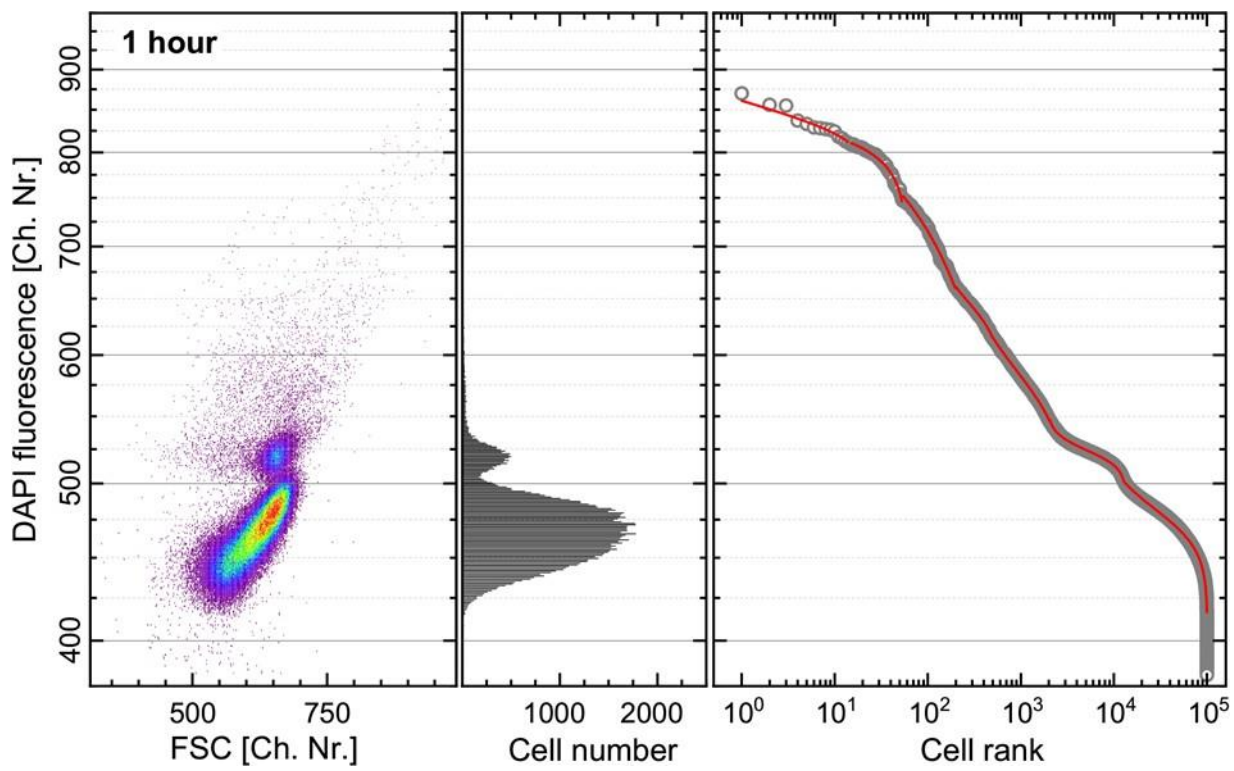
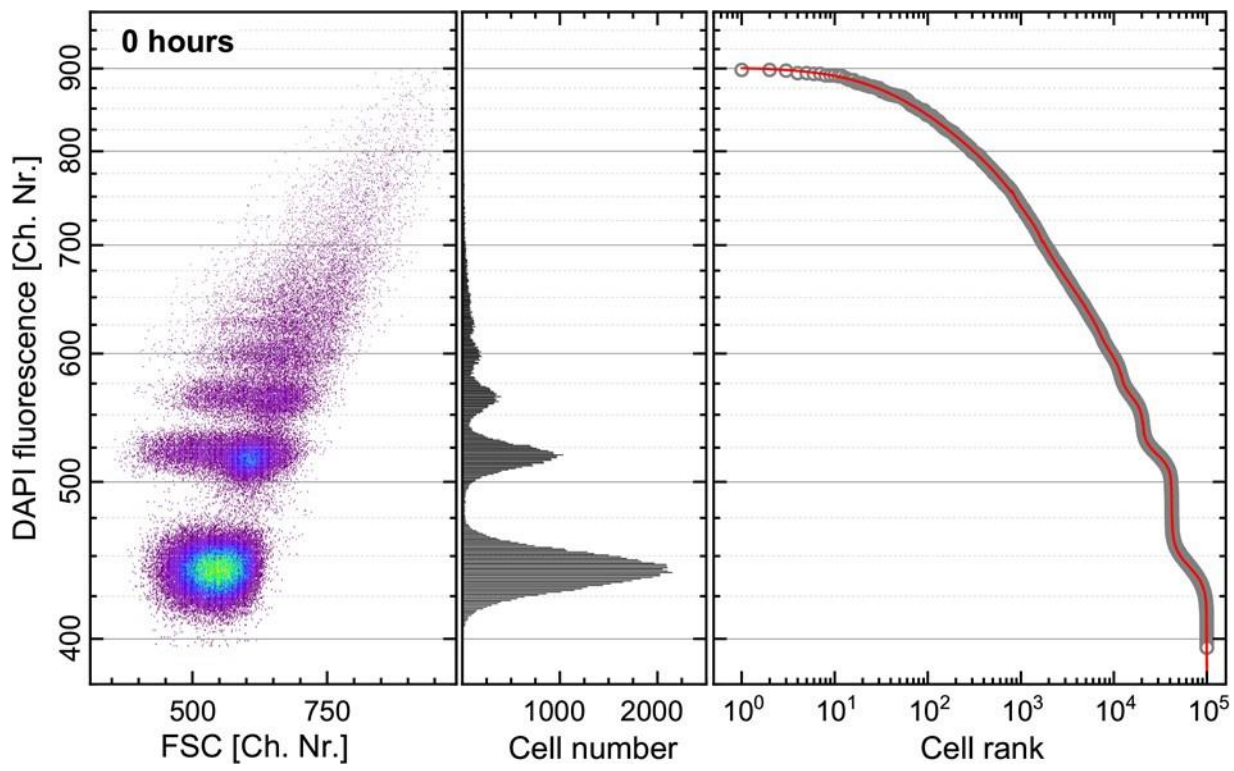
excluded from the calculation of the corresponding CDTI value.

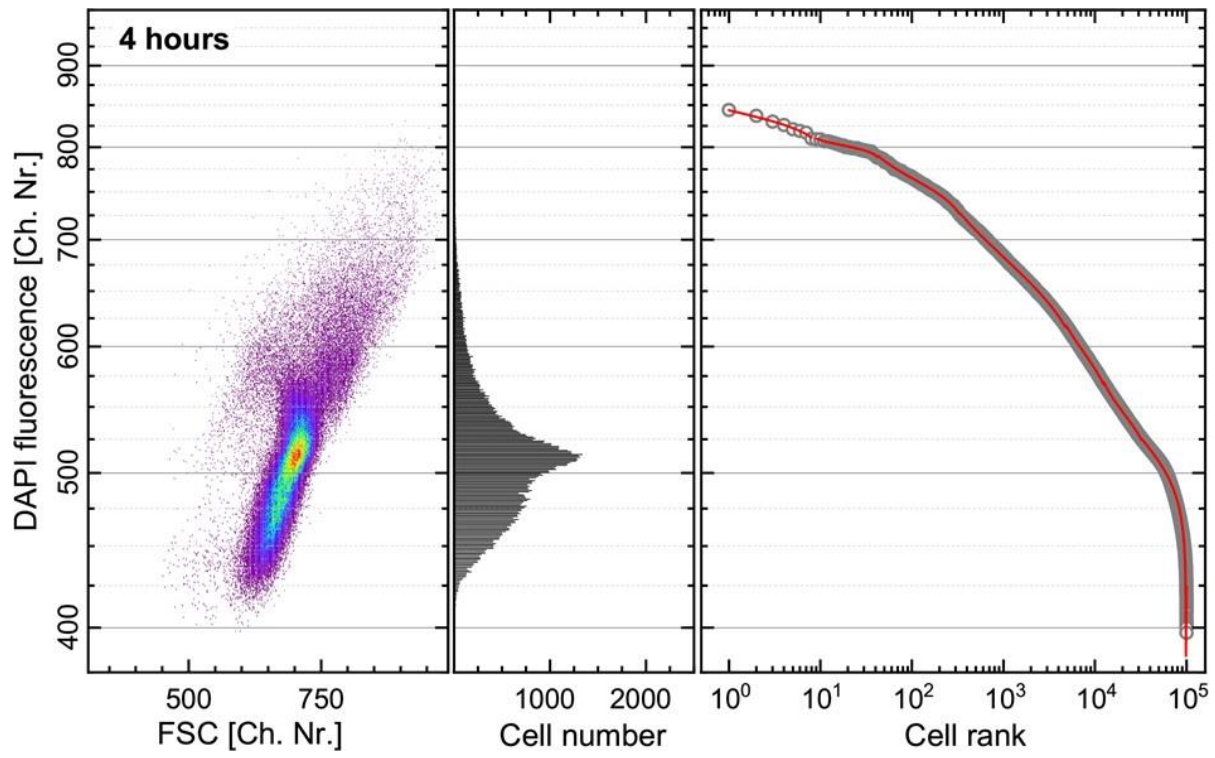
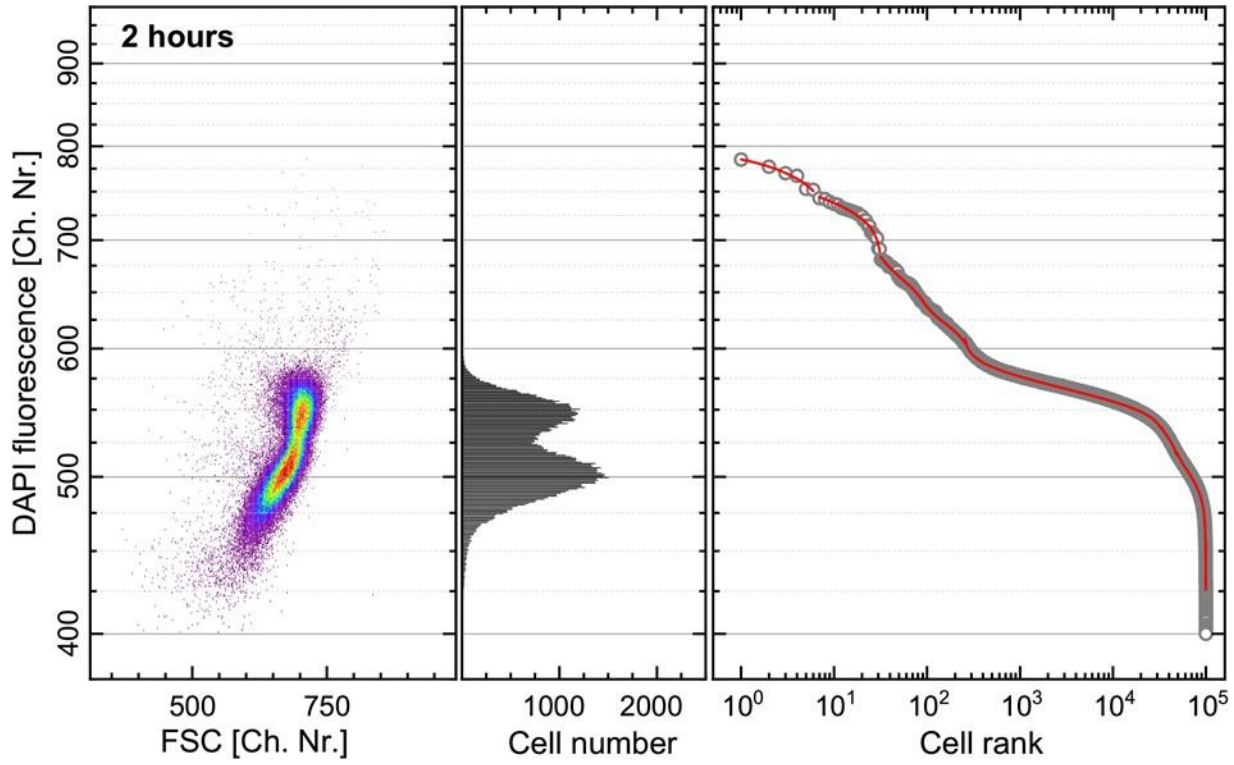


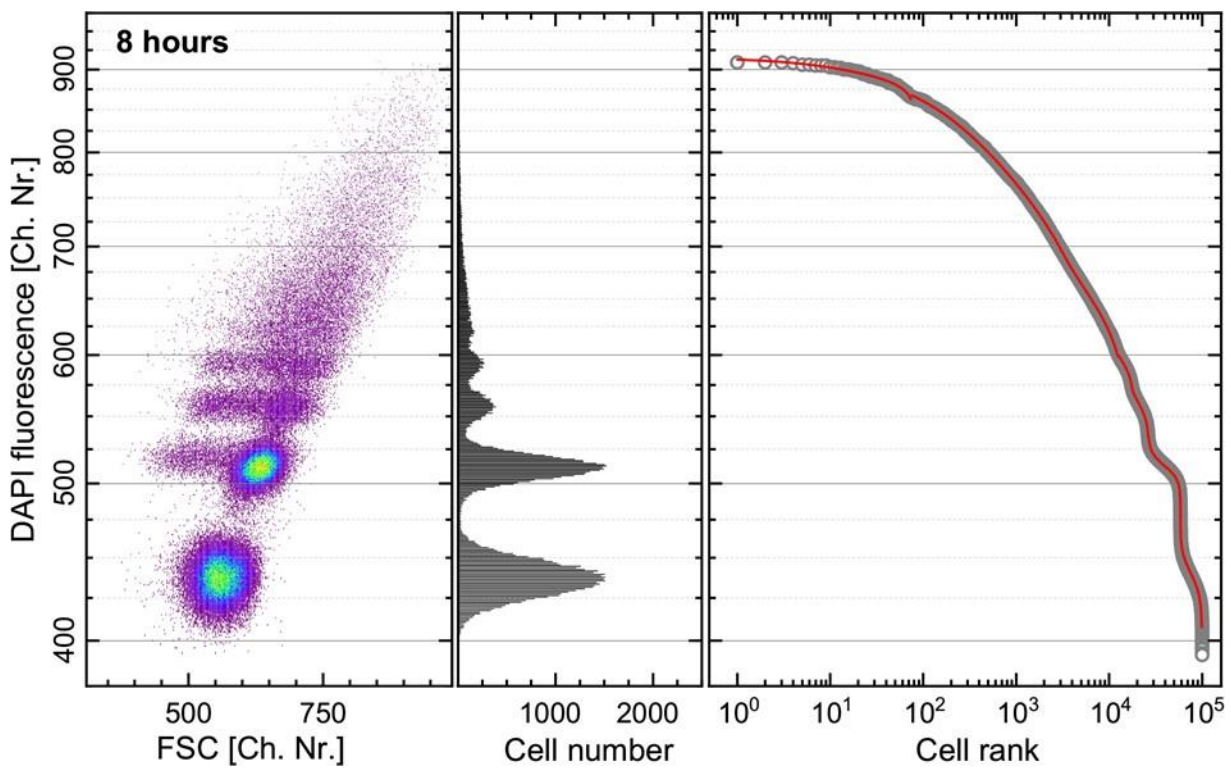
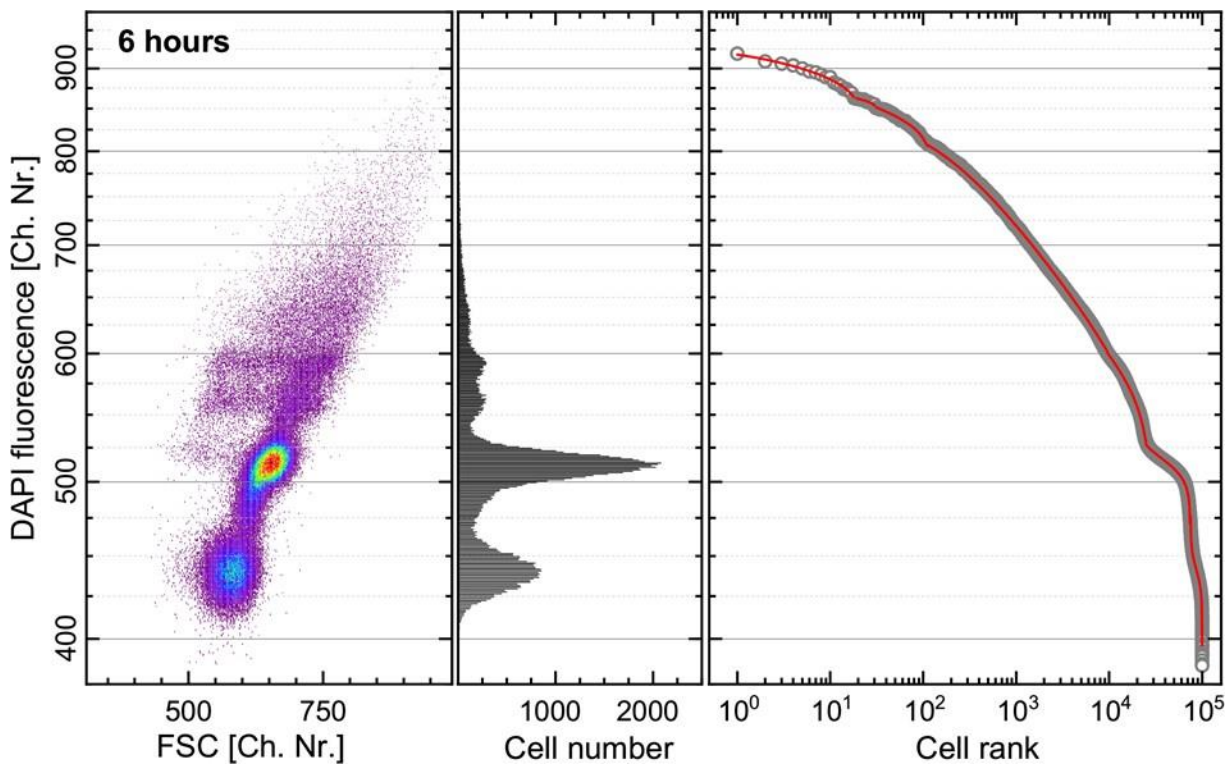
Supplementary Figure S10. The comparison of heterogeneity in anabolic activity of *P. putida* and *P. stutzeri* strains represented as CDTI trends over time.

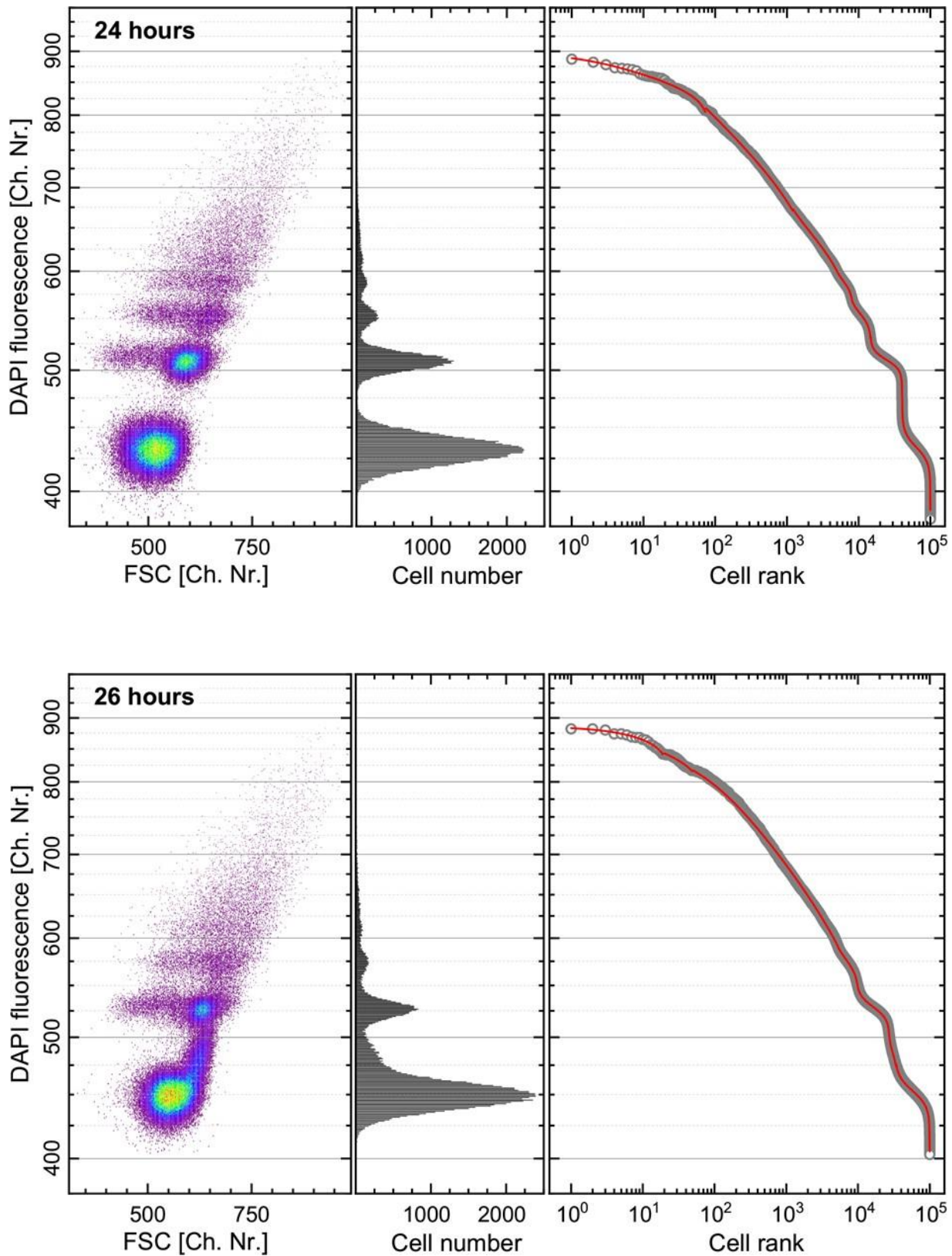


Supplementary Figure S11. Transformation of flow cytometric data prior to Zipfian approximation. The procedure was exemplarily visualized on the data acquired on *P. putida* cells at 0 h time point. 10^5 DAPI-stained cells were measured in logarithmic amplification mode and visualized in a forward scatter intensity (FSC, related to cell size) vs. DAPI fluorescence intensity (related to DNA content) dot plot (Frame A). Standard particle beads were measured with every sample to secure instrument stability. The events in the cell-gate were exported from the original .fsc files with the logarithmic scales of both axis evenly distributed into 1024 channels ranging from 0 to 1023 (Frame B). The boundaries between the five gates G1 to Gx were defined according to the local minima in the DAPI- fluorescence intensity distribution. In the last step, the range of DAPI-fluorescence intensity scale was confined within the cell-containing channels (channels: 375 to 975). This range was then represented on a warped scale to enhance resolution of the lower channel numbers where the majority of cells were measured (Frame C).









Supplementary Figure S12. Data of flow cytometry represented in dot plot, histogram and rank distribution of DAPI fluorescence intensity approximated with the multicomponent Zipfian function.